STM JOURNALS

Journal of
Polymer & Composites

ISSN: 2321-2810 (Online)
ISSN: 2321-8525 (Print)
Volume 14, Special Issue 1, 2026
DOI (Journal): 10.37591/JoPC

https://journals.stmjournals.com/jopc

Research JoPC

Dielectric Polymer Based Tunable Bandpass Filter for RF MEMS Applications

G.V. Ganesh[1,*], Nagandla Prasad[2], Pokkunuri Pardhasaradhi[3], Devarapu Santosh[4]

Abstract

In this paper, we report on the design, modeling, and analysis of a tunable bandpass filter implemented in a coplanar waveguide (CPW) configuration, where a distributed MEMS transmission line (DMTL) is integrated with dielectric polymer layers to achieve dynamic frequency and bandwidth reconfigurability. The proposed filter architecture leverages the tunable dielectric response of polymer films, enabling precise control of the center frequency and passband width under applied electrostatic bias. Comprehensive parametric studies were conducted on polymer characteristics—including dielectric constant, material selection, film thickness, surface uniformity, and air-gap geometry—to optimize capacitance variation, minimize actuation voltage, and maintain consistent RF stability. Electromagnetic simulations validated that the dielectric polymer integration allows center frequency tuning from 0.2 to 1 GHz, bandwidth reconfiguration of approximately 0.7 GHz, and superior microwave performance, characterized by a return loss of –22.5 dB and insertion loss near –3 dB. The fabrication process is compatible with low-temperature processing and flexible substrates, offering excellent scalability for compact and conformal microwave systems. Owing to its reconfigurable nature and reliable performance, the proposed dielectric polymer–based RF MEMS bandpass filter holds significant potential for next-generation UHF, radar, and consumer wireless communication applications.

Keywords: Coplanar waveguide (CPW), dielectric polymers, Distributed MEMS transmission layer, electromagnetic simulations, MEMS switches, parametric studies, reconfigurability, RF transmission

***Author for Correspondence**
G.V. Ganesh

[1]Associate Professor, Department of Electronics and Communication Engineering, Koneru Lakshmaiah Education Foundation, Vaddeswaram, Andhra Pradesh, India.
[2]Assistant Professor, Department of Electronics and Communication Engineering, GMR Institute of Technology, Rajam, Andhra Pradesh India.
[3]Professor, Department of Independent Research and Development and Electronics and Communication Engineering, Koneru Lakshmaiah Education Foundation, Vaddeswaram, Andhra Pradesh, India.
[4]Research Scholar, Department of Electronics and Communication Engineering, Koneru Lakshmaiah Education Foundation, Vaddeswaram, Andhra Pradesh, India.

Received Date: November 06, 2025
Accepted Date: January 19, 2026
Published Date: February 26, 2026

Citation: Devarapu Santosh, G.V. Ganesh1, Nagandla Prasad, Pokkunuri Pardhasaradhi. Dielectric Polymer Based Tunable Bandpass Filter for RF MEMS Applications. Journal of Polymer & Composites. 2026; 14(Special Issue 1): S1449–S1470p.

INTRODUCTION

Technology of Microelectromechanical systems (MEMS) devices that can pack mechanical and electrical components, e.g., sensors and actuators, on one substrate provide great potential for compact and effective multifunctional tools [1]. MEMS use is growing widely in such fields as biomedical, wireless communication, aerospace, and chemical processing. Among these, MEMS technology has recently received great interest in radio frequency (RF) applications. RF MEMS devices are used for switching, varactors, reconfigurable inductors and capacitors, and tunable filters and adaptive antennas. RF MEMS devices are becoming increasingly favored for high-performance, miniaturized RF systems due to their inherent advantages, such as low insertion loss, high return loss, a high Q factor, and ultra-low power consumption. Minimal usage of energy and materials, lesser cost, decrease in size and weight.

For the design of RF MEMS-based tunable band-pass filters, the choice of substrate and dielectric material plays a critical role in determining the overall electromagnetic performance, insertion loss, and thermal reliability of the device. Polyimide (PI), Liquid Crystal Polymer (LCP), and PVDF-TrFE are widely explored dielectric polymers due to their flexibility and compatibility with MEMS fabrication. Among these, LCP exhibits the most favorable high-frequency characteristics, with a low dielectric constant (≈2.9–3.2) and very low loss tangent (≈0.002–0.004), making it highly suitable for microwave and millimeter-wave applications. Polyimide, with a moderate dielectric constant (≈3.2–3.5) and slightly higher loss factor, offers exceptional thermal stability (Tg up to 400°C) and mechanical robustness, which is advantageous in MEMS structures exposed to harsh thermal cycles. In contrast, PVDF-TrFE provides a significantly higher dielectric constant (≈10–13), enabling enhanced capacitive tunability; however, its higher dielectric loss and lower thermal endurance (operating limit ~120°C) restrict its use in high-frequency, high-temperature RF environments. Overall, LCP is preferred for low-loss RF performance, PI is selected for thermally stable MEMS integration, and PVDF-TrFE is beneficial when high permittivity or electroactive behavior is required, depending on the filter's design priorities.

RF MEMS circuits are easily compatible with the microwave-integrated circuit through submissive fabrication methods and low IDM (inter modulation distortion) [2-8]. Reconfigurable RF circuits, which may alter circuit layouts in accordance with wireless standards without increasing the size or power consumption, would enable multiband operation. Wide range tunability of wideband oscillators is also advantageous [21]. Modern multiband and multifunction radios must meet several criteria, including fast bit rates, power tolerance, high resonance sharpness, broad frequency range, instantaneous tuning, uncorrupted signal, micro, and affordable. To carry out these duties, suitable RF transceivers are required [9]. One example is that a smartphone has Bluetooth and wireless LAN capabilities in addition to 3G/4G connections. As the number of required frequency bands increases, the total number and cost of discrete microwave filters (such as those used in multi-band radios) also rise. A single lightweight tunable filter has advantages over multiple big separate filters in terms of decreased weight, smaller integration, increased performance, and higher adaptability. In the beginning, scientists employed hollow metal waveguides with trimming screws or mechanically tunable coaxial lines. Electronically adjustable or tunable devices for RF systems have advanced significantly over the past ten years [37, 39]. Mechanically adjustable devices offered low-loss solutions and were simple to use. However, they required high-power control because they were large, expensive, sluggish, and vibration sensitive. Other tuning technologies that are either electrically, magnetically, or both electrically and magnetically tunable are now replacing these mechanically tunable filters. Either continuous or discrete states are employed in electronic tuning. PIN diodes and MEMS switches, among other devices, can be used to provide discrete tuning states [27, 28, 40, 42, 44, 45, 47-56]. Continuous tuning, as a secondary tuning method, can be achieved using MEMS capacitors, varactor diodes, ferromagnetic materials, or ferroelectric materials. MEMS switches and varactors have gotten a lot of interest recently. These devices promise to operate better than bulk devices due to high linearity, low power consumption and low losses.

In the previous works, varactor diodes are placed at the ends of the resonating stubs to get tuned to the center frequency [10]. [11-12] investigated both center frequency and bandwidth tuning utilizing hairpin resonators and combining structures. [13] Described a band stop filter that can tune both the center frequency and the bandwidth. Non-linearity is evident in varactor diodes, according to the literature review. A Bandpass filter that changes between 0.5 GHz and 2 GHz center frequencies was shown using PIN diodes [14]. A coplanar waveguide (CPW) with periodic structures which uses MEMS switches for tuning was presented in [15]. By using MEMS cantilever switch both bandwidth and frequency tunable filter was studied in [16]. [17] described a bandpass filter using a MEMS switch and a series etched gap in the CPW structure with a center frequency of 10-13.5 GHz. Design and manufacturing of an RF MEMS adjustable band-pass filter with center frequency and bandwidth flexibility.

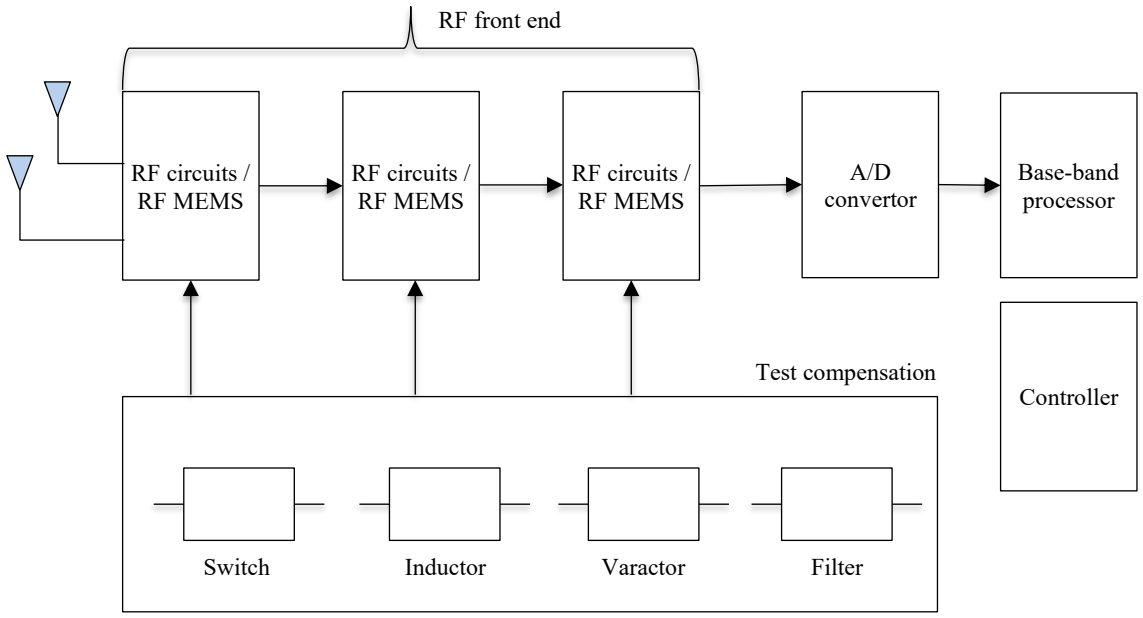

Figure 1. RF-MEMS device-based rf receiver block diagram

The topic of tuning is discussed in [18]. In comparison to other reconfigurable circuits, RF MEMS-based reconfigurable circuits are receiving a lot of interest. Several RF MEMS-based reconfigurable circuits have been built in recent years [29-36, 41-43, 45-48, 50]. In recent years several RF MEMS switches have been implemented [22-26]. The material selection for the RF MEMS switches is introduced in [20]. Figure 1 displays the block diagram of an RF transceiver using RF MEMS components [21]. RF transceivers are made up of several LSI chips as well as several off-chip passive components. Antennas, RF front end circuits, A/D converter, base band processor, and controller are shown in the block diagram. The RF frontend circuits are integrated with RF MEMS devices such as switches, filters, varactors, and inductors. Tunability and multiband operation are features of RF MEMS devices. MEMS switches can adapt a circuit to the desired frequency and bandwidth based on the communication band.

Extensive research on RF MEMS has addressed structural design, material selection, fabrication processes, and theoretical modeling. Notable contributions include the development of double-clamped beam switches on flexible liquid crystal polymer (LCP) substrates [57], RF MEMS switches on FR-4 organic substrates fabricated using wafer transfer technology (WTT) [58], thin-film silicon beam micro-resonators integrated onto low-temperature-processed polyethylene terephthalate (PET) substrates [59], and double-clamped beam resonators realized on ultrathin (10 μm) polyimide substrates [60]. Figure 1 illustrates RF-MEMS device-based RF receiver block diagram.

In this paper a distributed MEMS transmission line was used for the design of reconfigurable BPF. With the help of electrostatically actuated switches tunability can be achieved. Section 2 mainly presents the DMTL based filter structure and switches structures. The theoretical parameters of the switches are also covered in this section. Section 3 presents the optimization of proposed switches and filter by varying different parameters along with filter performance and Section 4 concludes the paper.

PROPOSED DESIGN

Proposed DMTL Tunable Bandpass Filter Structure

Figures 2 and 3 depict the suggested filter's schematic and top view, respectively. Table 1 lists the dimensions of the filter.

Table 1. Proposed dimensions for the filter.

S. No	Name of the parameter	Dimension (μm)
1	Length (L)	1467
2	Thickness of Ground line	1.5
3	Gap (G)	80
4	Width of Ground line (W)	100
5	Dielectric polymer Thickness (t_d)	.22
6	Thickness of Substrate	280

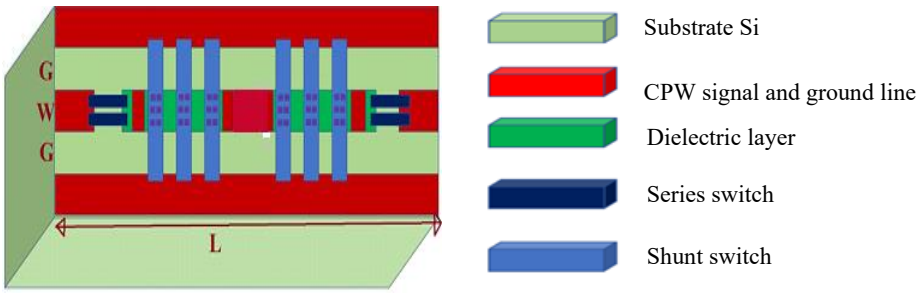

Figure 2. Proposed Filter illustration with different colors.

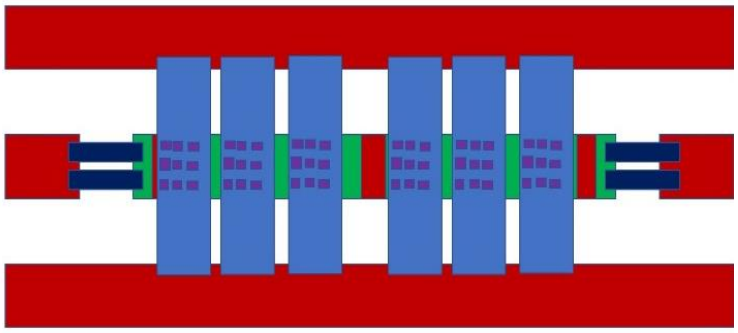

Figure 3. Top view illustration of proposed filter.

The construction is a CPW, with a communication line that terminates. Silicon is used as the substrate. A 220 nm-thick insulation layer is placed above the signal line to prevent the membrane from making direct contact with the underlying substrate.

Structure of RF MEMS Switches

The schematics for the switches used in the filter design are shown in Figures 4 and 5. The structural properties of the switches are summarized in Table 2. Four series (cantilever type) are positioned between the two discontinuities on either side of the signal line. On one side of the signal line, the cantilever is fixed by an anchor and moveable. We chose electrostatic actuation because it provides several benefits over alternative actuation technologies A cantilever type switch works by being in the up state (OFF state) at first, which prevents any signal from flowing to the opposite side. Applying voltage causes it to enter the down state (ON state), which enables the signal to pass through to the other side.

As capacitance between the top and bottom electrodes varies by changing the cantilever switch placements, most of the frequencies can be stopped so that the bandwidth can be adjusted. Shunt switches are placed on the groundlines with the help of anchors. It is initially in the up state (ON state) because there is no initial actuation voltage, which results in the output being an exact duplicate of the input. When there is a voltage differential between the two electrodes, the switch enters a down (OFF state) state and stops the signal [22–25].

Table 2. Proposed structural parameters for the switch.

S. No	Name of the parameter	Dimension (µm)
1	Series switch Beam length	94
2	Series switch Beam Width	30
3	Series switch Beam thickness	1.5
4	Air gap(g_0)	2
5	Shunt switch Beam Length	320
6	Shunt switch Beam Width	50
7	Shunt switch Beam Thickness	1.5
8	Perforation Width	15
9	Perforation length	15

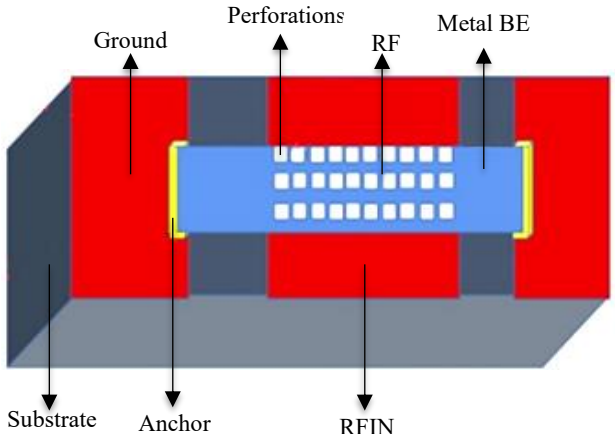

Figure 4. Diagram of a fixed-fixed switch.

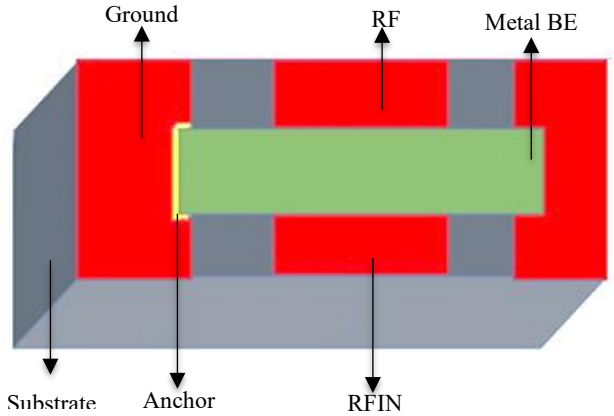

Figure 5. Diagram of a cantilever switch.

It offers great isolation at microwave frequencies when the beam is shut off, and the capacitance change is substantial. The fixed-fixed beam's bulk has been decreased via perforations. Accelerating switching, enhancing membrane flexibility, and reducing any residual tension on the beam are the primary goals of adding perforations to the beam. It also has an impact on the pull-in voltage. The top membrane's perforations lessen the up-state capacitance. The capacitance ratio influences any switch's insertion losses as the up-state capacitance decreases. These switches' primary functions are to modify the mid-frequency arrangement. The filter's frequency can be adjusted by changing the shunt capacitors' heights.

Table 3. Theoretically calculated values for both types of switches.

Parameter	Shunt switch	Series switch
Mechanical force constant	26.73N/m	6.42N/m
Electrical actuation voltage	15V	22 V
Switching time	24 us	14.7 us
On-state capacitance	3.65 pf	3.95 fF
Off-state capacitance	44 fF	0.29 pF

Structure of RF Mems Switch

This section gives an overview of the different parameters involved in designing any RF MEMS switch. The parameters are taken from [19].

Mechanical Force Constant

Membrane in fixed-fixed condition

$$k = 32Ew(t/l)^3$$

For cantilever membrane

$$k = \frac{2}{3}Ew(t/l)^3 \qquad (1)$$

Electrical Voltage for the actuation

$$v_p = \sqrt{\frac{8kg^3}{27\varepsilon A}} \quad (2)$$

Electromechanical Switching Time

$$t_s = 3.67\frac{V_p}{V_s w_0} \qquad (3)$$

$$w_0 = 2\pi f_0 \quad (4)$$

$$f_0 = 1.03\sqrt{\frac{E}{\rho}}\frac{h}{l^2} \qquad (5)$$

OFF state and ON state capacitance

$$C_{up} = \frac{(\varepsilon_0 A)}{\left(g+\frac{t_d}{\varepsilon_r}\right)} (6)$$

$$C_d = \frac{(\varepsilon_0 \varepsilon_r A)}{t_d} \quad (7)$$

The Theoretically calculated values for both types of switches are shown in the following Table 3.

RESULTS & DISCUSSION

Electromechanical Performance Optimization

Electromagnetic simulations were performed in a 3-D frequency-domain solver. The geometry given above has been implemented. A frequency sweep of 1–20 GHz (201 points) with adaptive mesh refinement was used. Radiation boundaries (PML) were placed ≥λ/4 from the device. Wave ports with 50 Ω reference impedance were used for excitation. The EM model was updated to obtain S-parameters vs bias. Mesh convergence was verified until the capacitance changed by <0.5% between refinements.

Materials selection for both conductor and insulating layer is the first thing to be considered. Because it decides the quality factor (Q). Q is inversely proportional to resistance. A graph among $\sqrt{E}$ and ρ^{-1} gives the materials selection (Figure 6). High $\sqrt{E}\rho^{-1}$ shows materials are Al, Au, Cu, Mo, Ir, Rh, W, Pt, and Ni. numerals in square brackets—e.g., [1] or [2, 3], or [4–6].

Aluminum has a lower electrical actuation voltage than Ni, which has the highest electrical actuation voltage. We can choose Cu in the middle because copper has a higher conductivity than Aluminum. When compared to other materials, Aluminum and nickel have the fastest switching speeds. Ni is the finest choice for a high E value and ultimate tensile strength.

To get a lower voltage pull, lower E and v values are required. When considering E and the mass density of all materials, copper has a high mass density. When all the above factors are considered, Aluminum is a fantastic choice for a conductor.

Figure 6 illustrates the ρ vs E for different materials. Using the COMSOL software, an electromechanical study is performed to assess the performance of our device. At first, we used FEM method to plot the pull in graphs by choosing gold, Si and Si_3N_4 as dielectric polymer, substrate, and conductors respectively.

Next step is to draw the pull in graphs by fixing the substrate, conductors and by taking Si_3N_4, SiO_2, and HfO2as dielectric polymer materials for both series and shunt. From these graphs we have chosen the dielectric polymer material. Next this procedure is repeated by fixing substrate and dielectric polymer for choosing the conductor material.

Shunt Switch

Out of three conductor materials chosen aluminum takes the less voltage to displace to the 2/3 of the gap (initially it is 2μm) which is as shown in Figure 7. Next by fixing the conductor as aluminum we plot the graphs for dielectric polymer variations. Out of three dielectric polymer materials chosen Si_3N_4 takes the less voltage to displace to the 2/3 of the gap (initially it is 2μm) which is as shown in Figure 8. Finally, we have taken aluminum and Si_3N_4 materials as metal and insulator respectively.

RF performance analysis of shunt switch is simulated from 0-5 GHz. Return loss varies from -0.035 to -0-005 within the frequency range as displayed in Figure 9. $S_{21}$is below -11dB as shown in Figure 10.

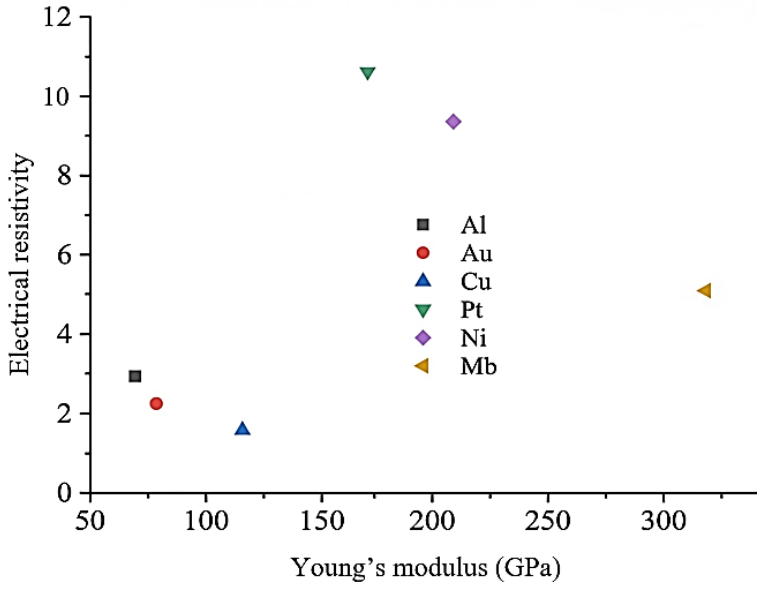

Figure 6. ρ vs E for different materials.

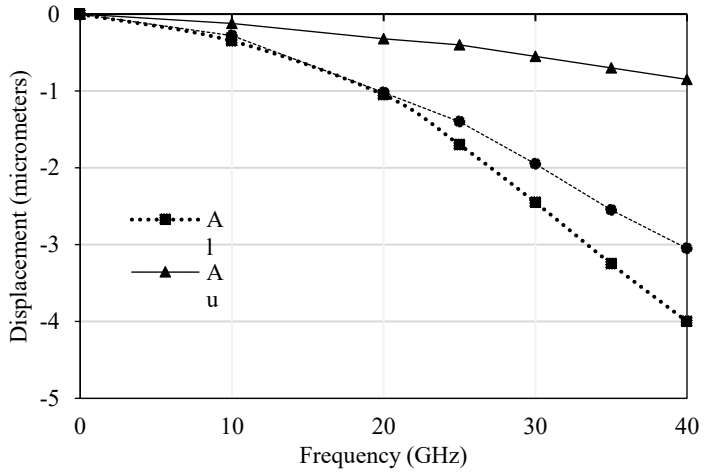

Figure 7. Pull in analysis graphs for three conductors.

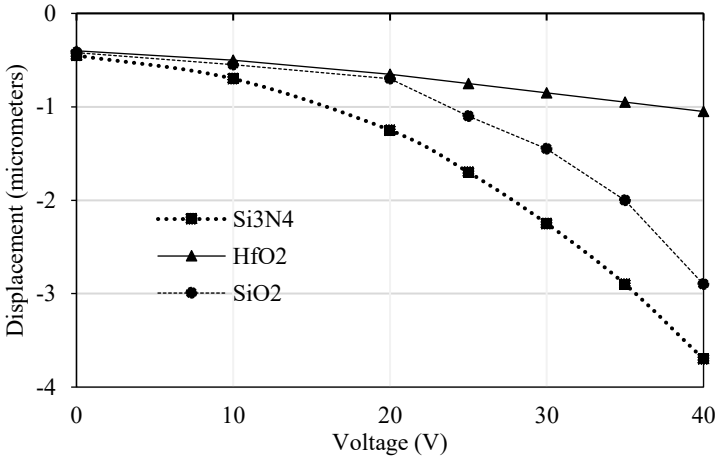

Figure 8. Pull in displacement comparison of 3 dielectric polymers.

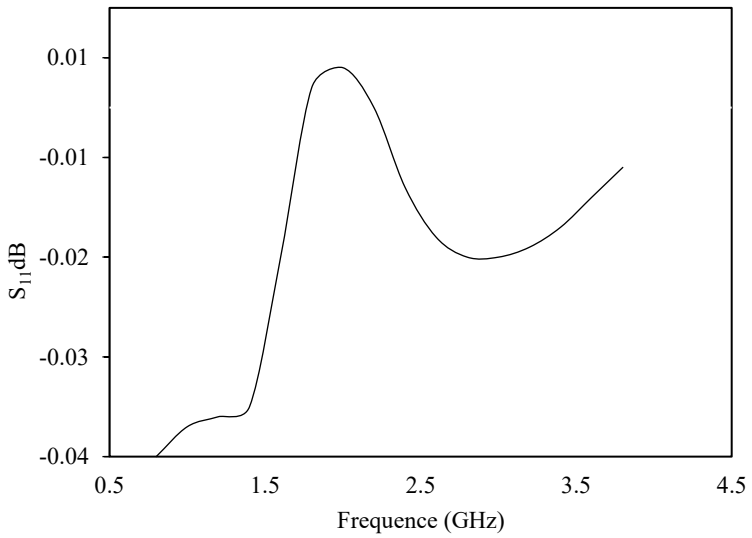

Figure 9. Return loss (S_{11}) in dB for shunt switch.

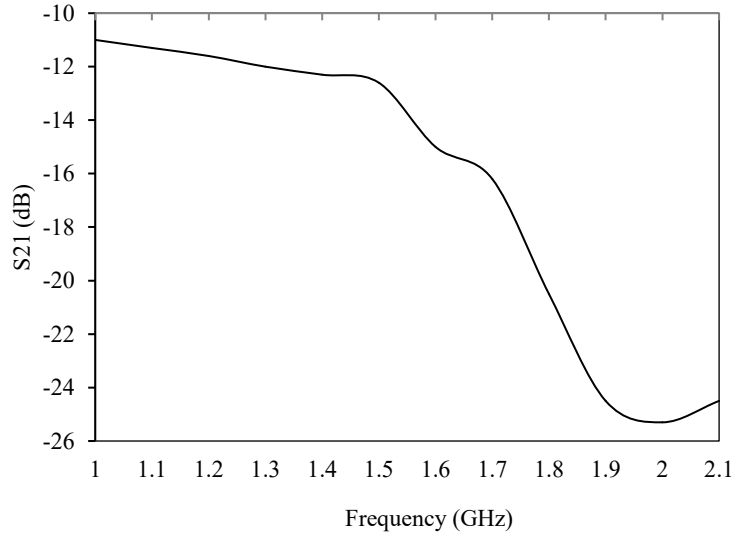

Figure 10. Insertion loss (S_{21}) in dB for shunt switch.

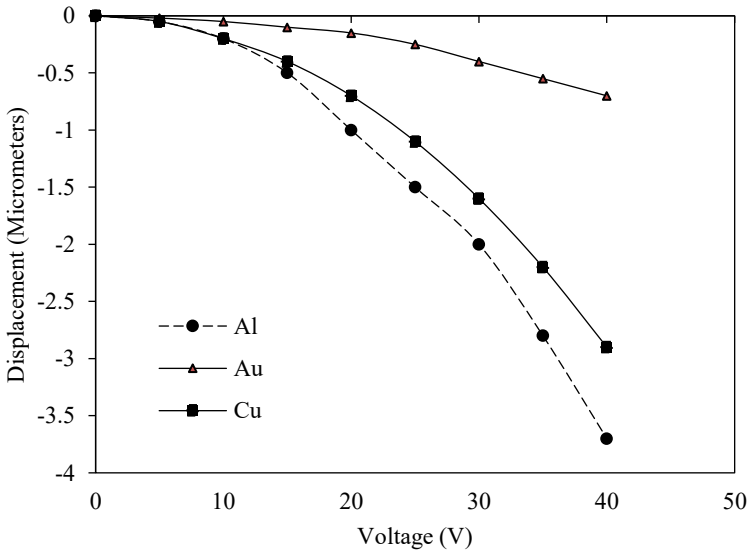

Figure 11. Pull in analysis graphs for three conductors.

Series Switch

Out of three conductor materials chosen aluminum takes the less voltage to displace to the 2/3 of the gap (initially it is 2μm) which is as shown in Figure 11. Next by fixing the conductor as aluminum we plot the graphs for dielectric polymer variations. Out of three dielectric polymer materials chosen Si_3N_4 takes the less voltage to displace to the 2/3 of the gap (initially it is 2μm) which is as shown in Figure 12. Finally, we have taken aluminum and Si_3N_4 materials as metal and insulator respectively.

RF performance analysis of cantilever type switch is carried out from 0-5 GHz. Return loss varies from -0.0725 to -0-0090 within the frequency range as shown in Figure 13. Insertion loss is below -15 dB as shown in Figure 14.

The selected dielectric materials will be integrated into the MEMS filter structure through a sequence of microfabrication steps optimized for compatibility with RF performance requirements. Dielectric material must spin-coated onto the substrate to form a uniform dielectric layer, followed by soft baking,

imidization curing, and patterning using standard photolithography. After which, via openings and metallization will be defined using laser micromachining and sputtering. A solution-processed thin film will be deposited through spin-coating and annealed to achieve the β-phase necessary for enhanced dielectric properties before electrode formation. In all cases, the metallization layers will be deposited using sputtering and patterned through lift-off to create the RF transmission lines, capacitive structures, and tunable elements of the filter.

Finally, the completed dielectric-metal stack will be released using a backside etch to form the suspended MEMS structures. This integrated process ensured low dielectric loss, mechanical stability, and compatibility with RF MEMS manufacturing flows.

Electromagnetic Performance Optimization

In this section optimization of the filter electromagnetic behaviour is done by varying different parameters of the device through simulator.

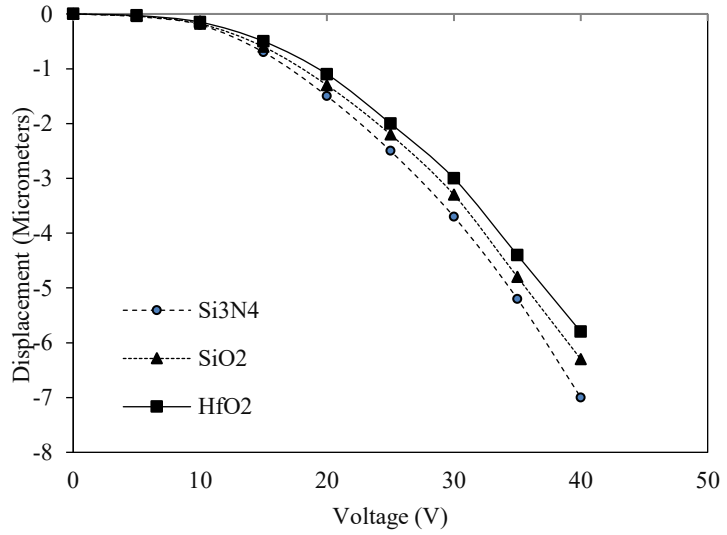

Figure 12. Pull in analysis graphs of three dielectric polymers.

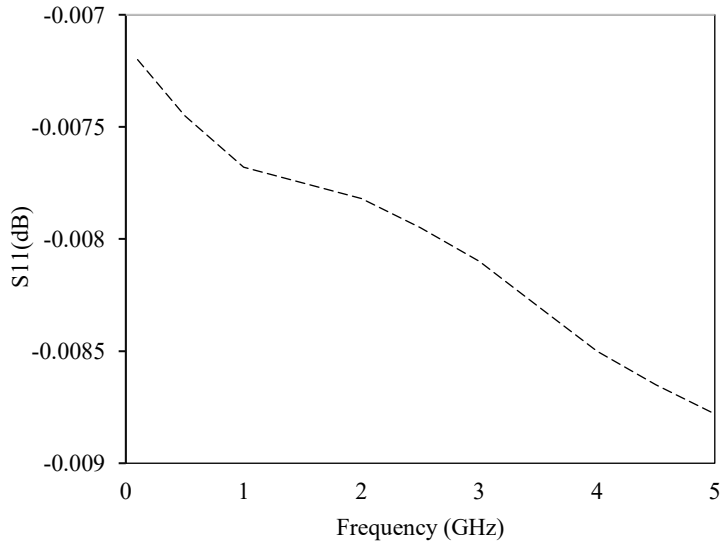

Figure 13. Return loss (S_{11}) in dB for Cantilever beam.

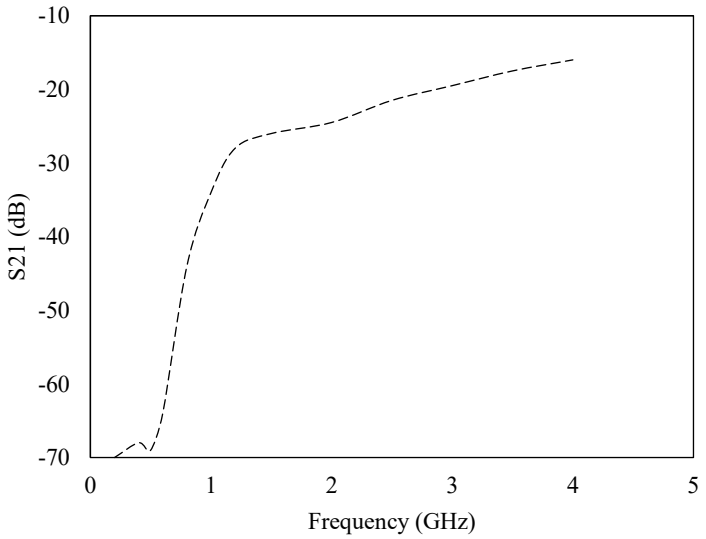

Figure 14. Insertion loss (S_{21}) in dB for Cantilever switch

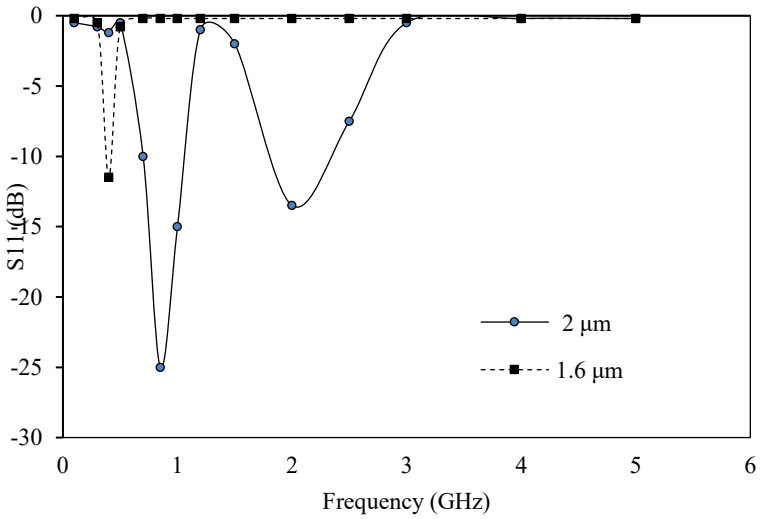

Figure 15. Variations of S_{11} parameter with air gap height variation.

Air Gap Height Optimization

Air gap is the one of the crucial factors for changing of the capacitance value. As capacitance changes the centre frequency changes. To get the less pull in voltage air gap should be less. Here we have done simulation for two air gap heights of 1.6 um and 2um, where 1.6um is the best to acquire less actuation voltage and required frequency.

Variations of S_{11} Parameter with air gap height Variation is shown in Figure 15. From the equations (6) and (7) there is an inverse relation between capacitance and air gap. So, as air gap reduces the capacitance value increases and frequency decreases so that centre frequency shifts to the left side. Finally, to get the centre frequency of 0.4 GHz we must choose the air gap of 1.6um.

Beam Width Optimization

Beam width is also affecting the centre frequency indirectly. Pull in voltage is depends on the beam width. But as beam width decreases switching time will reduce to the lesser value. As we change the beam width there is a slight change in the area, and it interns changes the capacitance and inductance. As beam width increase capacitance and inductance increases so that it decreases the centre frequency.

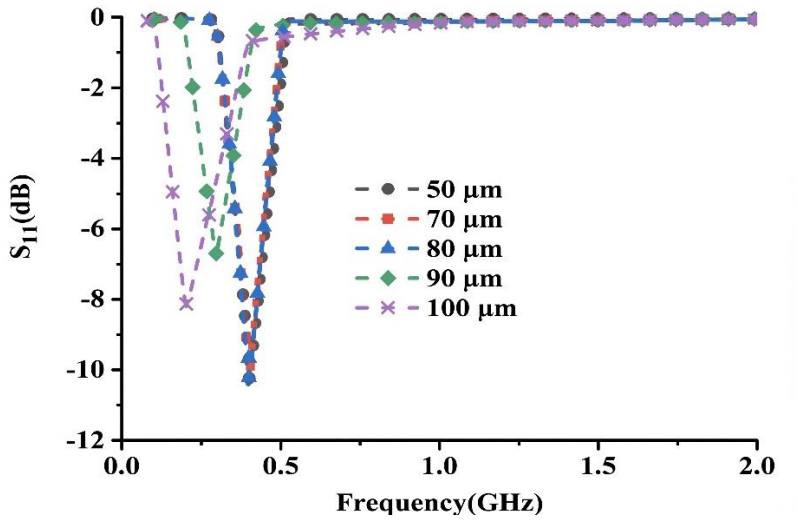

Figure 16. S_{11} Graph for variation in membrane width.

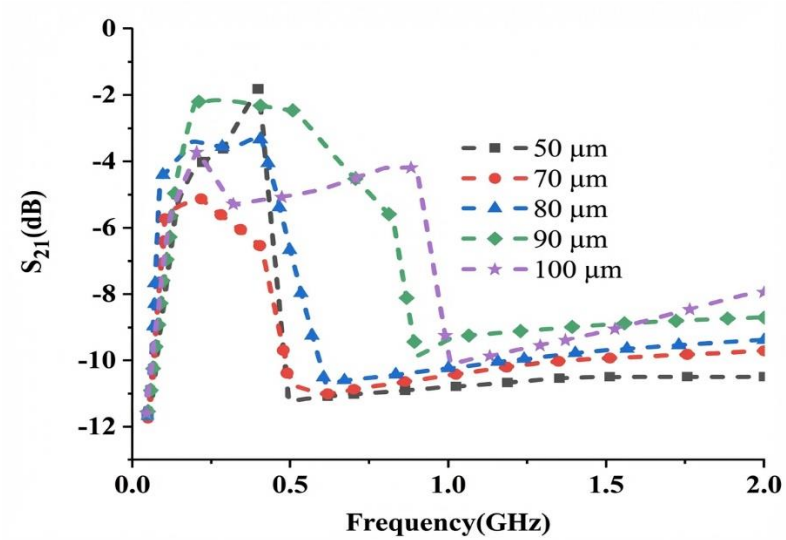

Figure 17. Variation of S_{21} for membrane width variation.

Figure 16 & 17 illustrates how the center frequency changes with a change in beam width (50µm to 100µm) for a fixed gap height. The central frequency decreases with the increase of the half wire-width. For example, with a 50µm beam width the center frequency is 0.4GHz and the S_{11} measurement is -11dB.

Dielectric Polymer Layer Material Properties Comparison

From the equations (6) and (7) dielectric polymer layer plays the vital role in the centre frequency change. The pull-in voltage and switching time are influenced by the dielectric polymer constant of the material used. To get the required frequency we must carefully optimize the dielectric polymer material.

Figures 18 &19 how the filter response for three materials, SiO_2, Si_3N_4, and Al_2O_3. The recorded centre frequencies are 1, 0.4, and 1.5GHz. S_{11} values of these materials are –15dB, –11dB, and –12dB, and S_{21} values of those are –1dB (SiO_2 and Si_3N_4) and –4dB (Al_2O_3). Although the center frequency of Al_2O_3 is very high, Al_2O_3's silicon compatibility is limited. From a performance and integration standpoint, Si_3N_4 serves as an excellent dielectric polymer, offering a reduced insertion loss, low resonant frequency, and improved return loss.

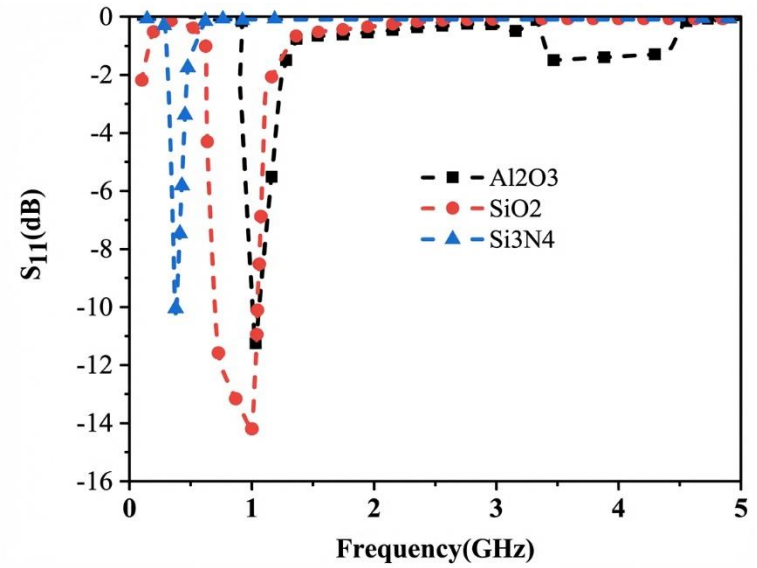

Figure 18. Change of S_{11} with dielectric polymer materials variation.

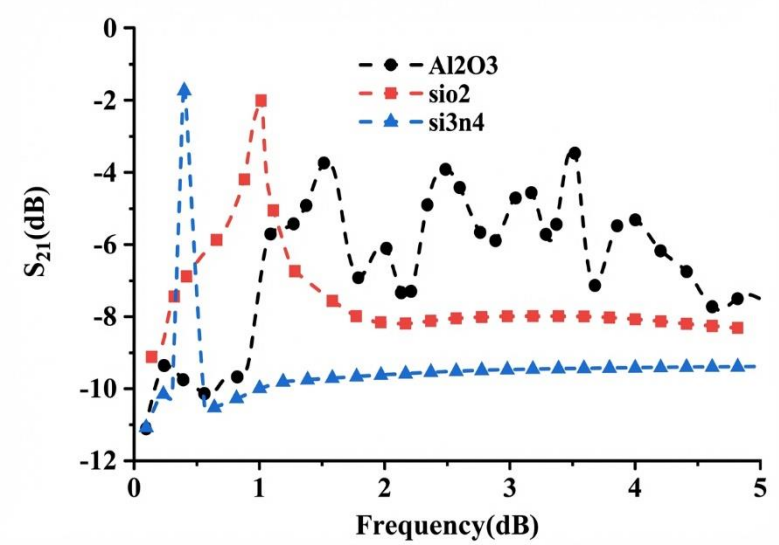

Figure 19. Change of S_{21} with dielectric polymer materials variation.

Optimization of Dielectric Polymer Thickness

The dielectric polymer layer thickness determines both the center frequency and the capacitances of the devices. For the smaller values, higher capacitance, lower center frequency as well as the lower frequency response shifts to the left. Meanwhile, thickening the insulation would sometime decrease the return loss. The effect of the dielectric polymer thickness of the S-parameters shows in figures 20 and 21. From this study the ideal thickness would be 0.2um.

Selection of Appropriate Substrate Material

Substrate also affects the center frequency. As center frequency is the function of the capacitance, if we increase capacitance, it will decrease the center frequency. Capacitance is the function of substrate dielectric polymer value. Figures 22 &23 shows the filter performance for six different substrate materials. Si is the best option as substrate at the centre frequency selected.

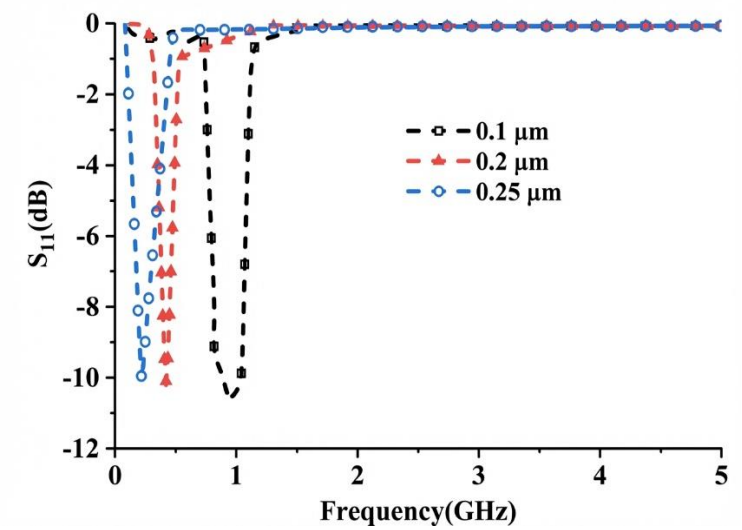

Figure 20. Change of S_{11} with dielectric polymer thickness variation.

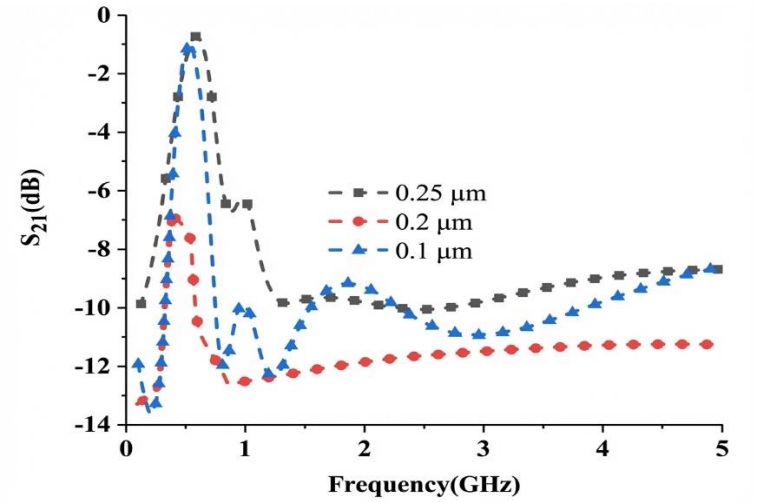

Figure 21. Change of S_{21} with dielectric polymer thickness variation.

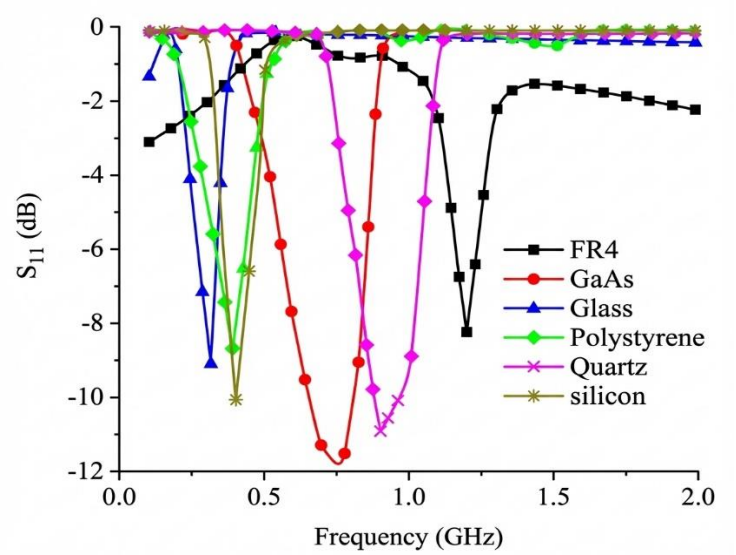

Figure 22. Change of S_{11} with substrate materials variation.

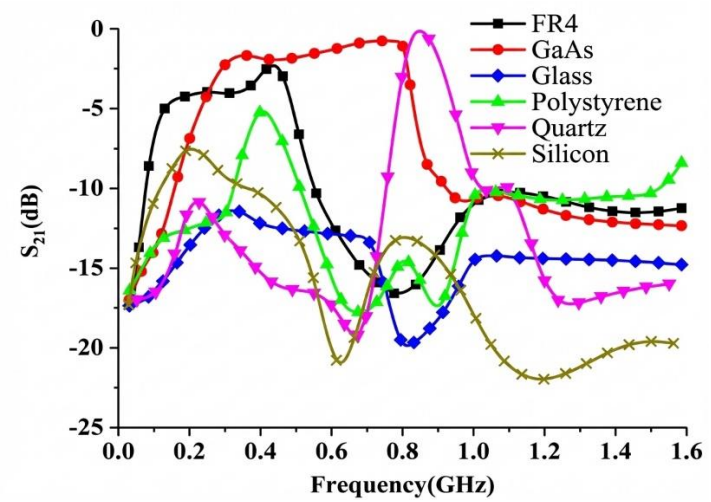

Figure 23. Change of S_{21} with substrate materials variation.

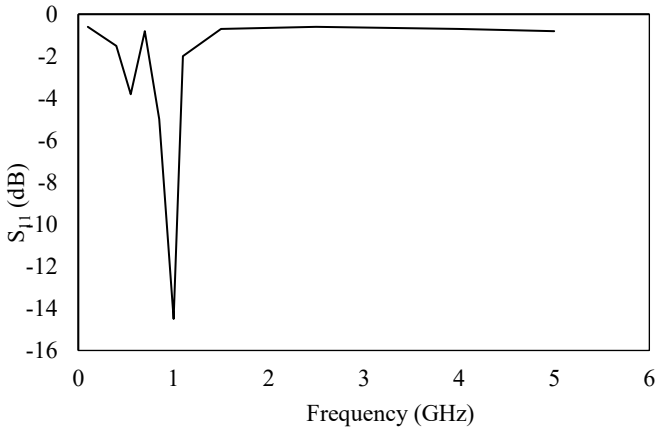

Figure 24. Proposed filter S_{11} in dB.

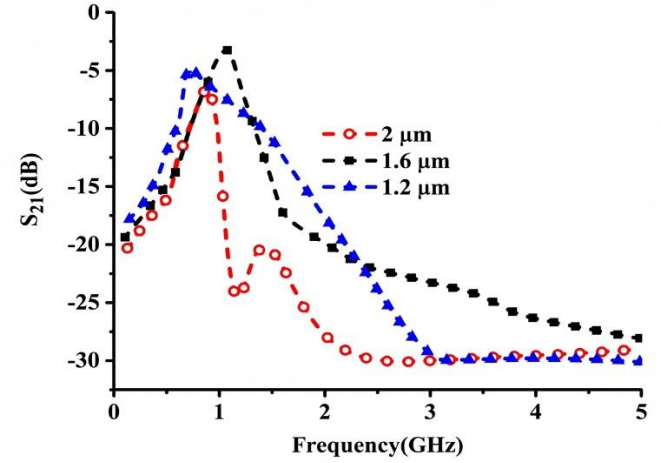

Figure 25. Proposed filter S_{21} in dB.

Performance of Filter

The S_{11} and S_{21} characteristics of the filters were analyzed using simulations under no actuation conditions. As depicted in figures 24 and 25, the designed filter demonstrates a band-pass behaviour, achieving approximately -6dB for S_{11} and -5dB for S_{21} at the design frequency of 1GHz.

The bandwidth of the coupling capacitor was adjusted while maintaining a constant shunt capacitance. As illustrated in figure 26, the bandpass filter exhibits a return loss of -11dB across the entire operational range. The 3dB bandwidth shown in Figure 27 is tunable from 0.3 GHz to 0.7 GHz. Throughout this range, the insertion loss S_{21} remains consistent at approximately -5dB.

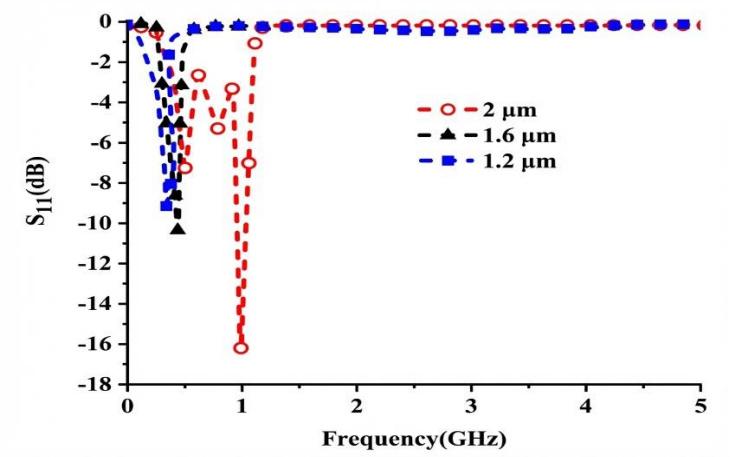

Figure 26. Center frequency shifts from 0.2 GHz-1 GHz.

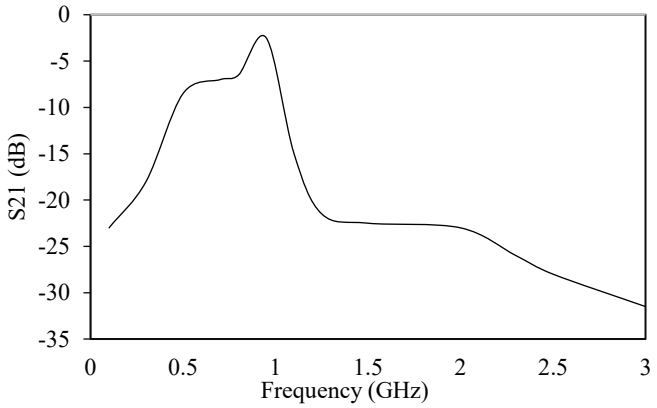

Figure 27. Change of S_{21} with the shift of center frequency.

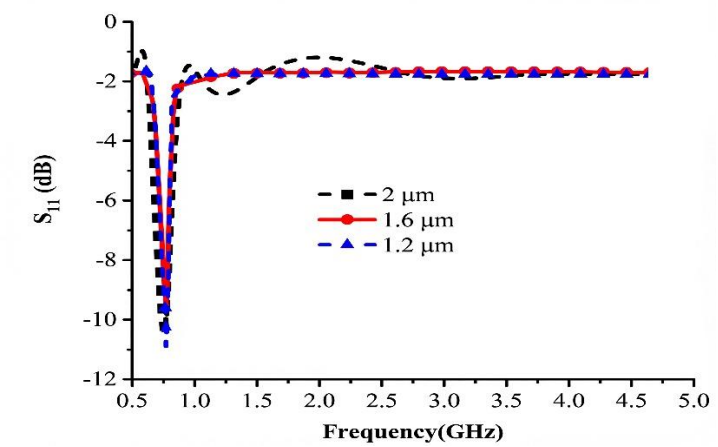

Figure 28. Change of S_{11} with the cantilever switch heights.

The coupling capacitor's bandwidth was tweaked while the shunt capacitance was fixed. As shown in Figure 28, the band-pass return loss across the entire operating range is -11 dB.

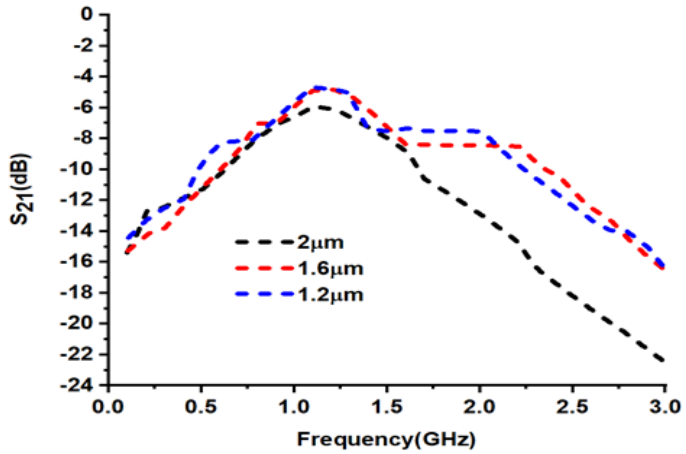

Figure 29. Change of S_{11} with the Cantilever switch heights.

The 3 dB bandwidth, illustrated in Figure 29, is tuned from 0.3 GHz (lower band) to 0.7 GHz (upper band). The bandpass S_{21} throughout the whole operational range is -5 dB.

Table 4. Comparison between comprehensive results with the filter proposed.

Implemented Parameter	Reference [18]	Reference [56]	Reference [17]	Reference [61]	Filter Proposed
Implementation of filter	Filter implemented with MEMS switch, series gap etched structure in coplanar waveguide (CPW).	Filter implemented with RF MEMS Switches and CSRR	Filter implemented with RF MEMS Switches and Open-Ring Resonators	MEMS capacitance switch and two resonant rings	Filter implemented with RF MEMS switches and DMTL
Change of Center frequency	10 GHz -13.5GHz	26.16 GHz -27.37 GHz	7.81 GHz -8.35 GHz	8.5–12 GHz	0.2 GHz -1GHz
Change of Bandwidth	----	------	----	---	0.7GHz
Change of Actuation voltage	23.5V	15.3V	26V	23V	15V(shunt), 22V(series)
Change of Bandpass Return Losses	−9 dB	-42.76 dB	∼−18 dB	∼−20 dB	∼−22.5 dB
Change of Bandpass Insertion Losses	−2.9 dB	-0.9 dB	∼−3.4 dB	∼1.12 dB	∼-3dB

Table 4. illustrates the Comparison between Comprehensive Results with Proposed filter. The proposed filter achieves optimal performance within the center frequency range of 0.2–1 GHz, delivering a return loss of -22.5 dB and an insertion loss of -3 dB across the bandpass spectrum.

CONCLUSION

This paper presents a new RF MEMS tunable bandpass filter that employs dielectric polymer films integrated within a distributed MEMS transmission line (DMTL) on coplanar waveguide (CPW) technology to achieve dynamic frequency tuning. A shunt-type capacitor using a polymer-based dielectric layer was designed, exhibiting tunable capacitances between 44 fF (low-bias state) and 3.65 pF (high-bias state) under an actuation voltage of 15 V. Similarly, a series capacitor incorporating a polymer dielectric achieved capacitances of 0.29 pF and 3.95 fF at an actuation voltage of 22 V. The use of dielectric polymers ensures stable performance across 0.1–3 GHz, while offering low-temperature process compatibility and mechanical flexibility. The device was further optimized to enhance passband characteristics, where the reconfiguration of the center frequency and bandwidth is governed by bias-induced changes in the polymer dielectric properties. The fabricated filter

demonstrates a tunable center frequency ranging from 0.2 to 1 GHz with a bandwidth adjustment of approximately 0.7 GHz. Excellent isolation was achieved, with return and insertion losses as low as –22.5 dB and –3 dB, respectively. Owing to its dielectric polymer–enabled tunability, low loss, and flexible integration, this filter is a strong candidate for UHF and emerging microwave communication applications.

Author Contributions

Devarapu Santosh: Conceptualization, methodology, simulation, data analysis, and manuscript drafting.

G.V. Ganesh: Supervision, guidance on experimental design, validation of results

Pokkunuri Pardhasaradhi: Critical review of the manuscript, manuscript revision for important intellectual content.

Nagandla Prasad: Resources, technical inputs, and manuscript revision for important intellectual content.

All authors have read and approved the final version of the manuscript.

Conflict of Interest

The authors declare that they have no known competing financial interests or personal relationships that could have appeared to influence the work reported in this paper.

Funding

This research received no specific grant from any funding agency in the public, commercial, or not-for-profit sectors.

REFERENCES

1. H. J. De Los Santos et al., “Introduction to Microelectromechanical (MEM) Microwave Systems”, Artech House, London, 1999.
2. Jason Yao, J. et al., “RF MEMS from a device perspective”, Rockwell Science Center. JMM engineering, 10, R9–R58, 2000.
3. Vu, T. M., Prigent, et al.,” The Design and fabrication of RF-MEMS switch for V-band reconfigurable application”, PIERS B, 39,301–318, 2012, doi: 10.2528/PIERB12021404.
4. S.Lucyszyn et al., “Radio frequency Microelectromechanical System”, IEEE Proc.-Sci. Meas. Technol. Vol. 151, No. 2, March 2004.
5. J.B.Muldavin et al., "High-Isolation Inductively tuned X-Band MEMS Shunt Switches", IEEE MTT-S International Microwave Symposium. Dig., Boston, Massachusetts, pp. 169- 172, USA, June 2000, doi:10.1109/MWSYM.2000.862109.
6. J. Y. Qian et al., "A Parametric Model of MEMS Capacitive Switch Operating at Microwave Frequencies", IEEE MTT-S Int. Microwave Symposium. Dig., Boston, Massachusetts, pp. 1229-1232, USA, June 2000, doi:10.1109/MWSYM.2000.862109.
7. J. B. Muldavin and G. M. Rebeiz, "30 GHz tuned MEMS switches," 1999 IEEE MTT-S International Microwave Symposium Digest (Cat. No.99CH36282), Anaheim, CA, USA, 1999, pp. 1511-1514 vol.4, doi: 10.1109/MWSYM.1999.780241.
8. J. Y. Park, G. H. Kim, K. W. Chung and J. U. Bu, "Fully integrated micromachined capacitive switches for RF applications," 2000 IEEE MTT-S International Microwave Symposium Digest (Cat. No.00CH37017), Boston, MA, USA, 2000, pp. 283-286 vol.1, doi: 10.1109/MWSYM.2000.860979.
9. Sulav Adhikari et al.,” Developing one-dimensional electronically tunable microwave and millimeter-wave components and devices towards two-dimensional electromagnetically

reconfigurable platform", Progress in Electromagnetics Research, Vol. 143, 821-848, 2013, doi: 10.2528/PIER13123006.
10. I. C. Hunter and J. D. Rhodes, "Electronically Tunable Microwave Bandpass Filters," in IEEE Transactions on Microwave Theory and Techniques, vol. 30, no. 9, pp. 1354-1360, Sep. 1982, doi: 10.1109/TMTT.1982.1131260.
11. Moon-Seok Chung, Il-Soo Kim and Sang-Won Yun, "Varactor-tuned hairpin bandpass filter with an attenuation pole," 2005 Asia-Pacific Microwave Conference Proceedings, Suzhou, China, 2005, pp. 4 pp.-, doi: 10.1109/APMC.2005.1606748.
12. M. Sanchez-Renedo, R. Gomez-Garcia, J. I. Alonso and C. Briso-Rodriguez, "Tunable combline filter with continuous control of center frequency and bandwidth," in IEEE Transactions on Microwave Theory and Techniques, vol. 53, no. 1, pp. 191-199, Jan. 2005, doi: 10.1109/TMTT.2004.839309.
13. Musoll-Anguian et al., "Fully adaptable band-stop filter using varactor diode," Microwave and Optical Technological Letters, Vol. 52, Mar. 2002, doi: 10.1002/mop.24969.
14. Brito-Brito, Z., et al., "Micro strip switchable BSF using PIN diodes with precise frequency and bandwidth control", Proceedings of EUMA, 1707-1711, 2008, doi: 10.1109/EUMC.2008.4751804.
15. Park, J.-H., et al., "Reconfigurable millimeter wave filters using CPW based periodic structures with novel multiple-contact MEMS switches", JMM, Vol. 14, No. 3, Jun.2005, doi:10.1109/JMEMS.2005.844849.
16. E. Fourn et al., "Bandwidth and central frequency control on tunable bandpass filter by using MEMS cantilevers," IEEE MTT-S International Microwave Symposium Digest, 2003, Philadelphia, PA, USA, 2003, pp. 523-526 vol.1, doi: 10.1109/MWSYM.2003.1210991.
17. N. Zhang, L. Mei, C. Wang, Z. Deng, J. Yang and Q. Guo, "A Switchable Bandpass Filter Employing RF MEMS Switches and Open-Ring Resonators," in IEEE Transactions on Electron Devices, vol. 64, no. 8, pp. 3377-3383, Aug. 2017, doi: 10.1109/TED.2017.2712643.
18. Naibo Zhang et al., "Design and Analysis of a Tunable Bandpass Filter Employing RF MEMS Capacitors", IEEE electron device letters, 2011, 32, pp. 1460-1462, doi: 10.1109/LED.2011.2162814.
19. S. C. Saha et al.," Tunable BPF using RF MEMS capacitance and transmission line," PIER C, Vol. 23, 2011, pp. 233-247, doi:10.2528/PIERC11070607.
20. G.M Rebeiz, RF MEMS: Theory, Design, and Technology; Wiley: NY, USA, 2003.
21. A.K.Sharma et al.," material selection of RF-MEMS switch used for reconfigurable antenna using Ashby's approach," PIERS, vol. 31, pp. 147-157, 2012, doi:10.2528/PIERL12021101.
22. Kei Kuwabara et.al," Integrated RF-MEMS Technology for Reconfigurable RF Transceivers," NTT Technical review, Vol. 5, No. 10, pp.1-6, Oct. 2007, doi: 10.53829/ntr200710sp4.
23. Yasser Mafinejad et al., "Design and simulation of a high isolation RF MEMS shunt capacitive switch for C-K band," IEICE Electronics Express, Vol.10, No.24, pp. 1–8, 2013, doi:10.1587/elex.10.24.2123.
24. Fang, D. M., Li, X. H., Yuan, Q., & Zhang, H. X. (2010). Effect of etch holes on the capacitance and pull-in voltage in MEMS tunable capacitors. International Journal of Electronics, 97(12), 1439–1448. Doi: 10.1080/00207217.2010.488911.
25. V. L. Rabinovich, R. K. Gupta and S. D. Senturia, "The effect of release-etch holes on the electromechanical behavior of MEMS structures," Proceedings of International Solid State Sensors and Actuators Conference (Transducers '97), Chicago, IL, USA, 1997, pp. 1125-1128 vol.2, doi: 10.1109/SENSOR.1997.635400.
26. Deshmukh D, Angira M (2019) Investigation on switching structure material selection for RF-MEMS shunt capacitive switches using Ashby, TOPSIS and VIKOR. Trans Electr Electron Mater 20(3):181–188, doi: 10.1007/s42341-018-00094-3.
27. Shanthi, G., Srinivasa Rao, K. & Girija Sravani, K. Design and analysis of a RF MEMS shunt switch using U-shaped meanders for low actuation voltage. Microsyst Technol 26, 3783–3791 (2020). Dpi: 10.1007/s00542-020-04864-z.

28. Shanthi, G., Srinivasa Rao, K., Girija Sravani, K. (2021). Electromagnetic Analysis of MEMS-Based Tunable EBG Band stop Filter Using RF MEMS Switch for Ku-Band Applications. In: Chowdary, P., Chakravarthy, V., Anguera, J., Satapathy, S., Bhateja, V. (eds) Microelectronics, Electromagnetics and Telecommunications. Lecture Notes in Electrical Engineering, vol 655. Springer, Singapore. Doi: 10.1007/978-981-15-3828-5_18.
29. Thalluri, L.N., Guha, K., Srinivasa Rao, K. et al. Perforated serpentine membrane with AlN as dielectric material shunt capacitive RF MEMS switch fabrication and characterization. Microsystem Technol 26, 2029–2041 (2020). Doi: 10.1007/s00542-020-04755-3.
30. Mahesh Kumar Chaubey and Avanish Bhadauria," RF MEMS Based Tunable Bandpass Filter For X-Band Applications", Materials Science and Engineering, Volume 331, 14–16 October 2017, doi: 10.1088/1757-899X/331/1/012030.
31. Hore S., Maity S., Sarma J., Choudhury A., Yadav G.," RF MEMS Based Band-Pass Filter for K-Band Applications", Advances in Intelligent Systems and Computing, 2016, vol 452., doi: 10.1007/978-981-10-1023-1_37.
32. Sifat, S.M., Savaj, R., Stiharu, I., Kishk, A. (2020). Wideband Bandpass Filter Design Based on RF-MEMS Technology. In: Gheorghe, G. (eds) Proceedings of the International Conference of Mechatronics and Cyber- Mix Mechatronics - 2020. ICOMECYME 2020. Lecture Notes in Networks and Systems, vol 143. Springer, Cham. doi: 10.1007/978-3-030-53973-3_20.
33. Sukomal Dey,Shiban K. Koul,Ajay K. Poddar,Ulrich L. Rohde," Frequency and bandwidth tunable reliable MEMS bandpass filter for 24 GHz radar applications", International Journal of RF and Microwave Computer-Aided Engineering, 2021, doi: doi.org/10.1002/mmce.22662.
34. Ngasepam Monica Devi, Santanu Maity, Rajesh Saha & Sanjeev Kumar Metya, "RF MEMS and CSRRs-based tunable filter designed for Ku and K bands application", Cogent Engineering,2015, doi: 10.1080/23311916.2015.1083641.
35. Syed M. Sifat, Raj Savaj, Ion Stiharu, Ahmed Kishk," WIDEBAND BANDPASS FILTER DESIGN BASED ON RF-MEMS TECHNOLOGY", International Journal of Mechatronics and Applied Mechanics, 2020, Issue 7, doi: 10.1007/978-3-030-53973-3_20.
36. S. M. Sifat, M. M. M. Ali, S. I. Shams and A. -R. Sebak, "High Gain Bow-Tie Slot Antenna Array Loaded with Grooves Based on Printed Ridge Gap Waveguide Technology," in IEEE Access, vol. 7, pp. 36177-36185, 2019, doi: 10.1109/ACCESS.2019.2902596.
37. S. Dey and S. K. Koul, "Reliable, Compact, and Tunable MEMS Bandpass Filter Using Arrays of Series and Shunt Bridges for 28-GHz 5G Applications," in IEEE Transactions on Microwave Theory and Techniques, vol. 69, no. 1, pp. 75-88, Jan. 2021, doi: 10.1109/TMTT.2020.3034182.
38. R. J. Cameron, C. M. Kudsia and R. R. Mansour, Microwave Filters for Communication Systems, Hoboken, NJ, USA: Wiley,2018.
39. F. A. C. S. Lucena, C. P. N. Silva, T. L. Pedrosa and M. T. de Melo, "Gain enhancement of dual-band antenna using square loop FSS," 2017 IEEE International Symposium on Antennas and Propagation & USNC/URSI National Radio Science Meeting, San Diego, CA, USA, 2017, pp. 2169-2170, doi: 10.1109/APUSNCURSINRSM.2017.8073127.
40. R. J. Cameron, C. M. Kudsia and R. R. Mansour, Microwave Filters for Communication Systems Fundamentals Design and Applications, Hoboken, NJ, USA: Wiley, 2018, DOI:10.1002/9781119292371.
41. W. Feng et al., "28-GHz High-Selectivity Bandpass Filters with Dual-Behavior Resonators Using GaAs Technology," in IEEE Transactions on Plasma Science, vol. 47, no. 12, pp. 5277-5282, Dec. 2019, doi: 10.1109/TPS.2019.2950708.
42. Y. Yang, X. Zhu and Q. Xue, "Design of an Ultracompact On-Chip Bandpass Filter Using Mutual Coupling Technique," in IEEE Transactions on Electron Devices, vol. 65, no. 3, pp. 1087-1093, March 2018, doi: 10.1109/TED.2018.2797304S.
43. Z. J. Hou, Y. Yang, X. Zhu, Y. C. Li, E. Dutkiewicz and Q. Xue, "A Compact and Low-Loss Bandpass Filter Using Self-Coupled Folded-Line Resonator with Capacitive Feeding Technique,"

in IEEE Electron Device Letters, vol. 39, no. 10, pp. 1584-1587, Oct. 2018, doi: 10.1109/LED.2018.2864597.

44. F. Sun, R. G-Garcia, X. Zhu, H. Zhu, Y. Yang and X. Tong, "Miniaturized millimetre-wave BPF with broad stopband suppression in silicon–germanium technology", IET Microw. Antennas Propag., vol. 14, no. 4, pp. 308-313, Jan. 2020, doi:10.1049/iet-map.2019.0835.
45. M. G. Bautista, H. Zhu, X. Zhu, Y. Yang, Y. Sun and E. Dutkiewicz, "Compact Millimeter-Wave Bandpass Filters Using Quasi-Lumped Elements in 0.13 μm (Bi)-CMOS Technology for 5G Wireless Systems," in IEEE Transactions on Microwave Theory and Techniques, vol. 67, no. 7, pp. 3064-3073, July 2019, doi: 10.1109/TMTT.2019.2895581.
46. H. Zhu, X. Zhu, Y. Yang, and Q. Xue, "Design of Wideband Third-Order Bandpass Filters Using Broadside-Coupled Resonators in 0.13- μ m (Bi)-CMOS Technology," IEEE Transactions on Microwave Theory and Techniques, vol. 66, no. 12, pp. 5593–5604, Dec. 2018, doi: 10.1109/TMTT.2018.2873342.
47. H. Zhu, Y. Yang, X. Zhu, Y. Sun and S. -W. Wong, "Miniaturized Resonator and Bandpass Filter for Silicon-Based Monolithic Microwave and Millimeter-Wave Integrated Circuits," in IEEE Transactions on Circuits and Systems I: Regular Papers, vol. 65, no. 12, pp. 4062-4071, Dec. 2018, doi: 10.1109/TCSI.2018.2839701.
48. S. Dey, S. K. Koul, A. K. Poddar and U. L. Rohde, "Reliable and Compact 3- and 4-Bit Phase Shifters Using MEMS SP4T and SP8T Switches," in Journal of Microelectromechanical Systems, vol. 27, no. 1, pp. 113-124, Feb. 2018, doi: 10.1109/JMEMS.2017.2782780.
49. Feng Sun, Roberto Gómez-García, Xi Zhu, He Zhu, Yang Yang, Xunqian Tong," Miniaturized Millimeter-Wave Bandpass Filter with Broad Stopband Suppression in SiGe Technology", IET Microwaves, Antennas & Propagation, 2020, Vol. 14 Iss. 4, pp. 308-313, https://doi.org/10.1049/iet-map.2019.0528.
50. Ali, M., Liu, F., Watanabe, A., et al.: First demonstration of compact, ultra-thin low-pass and bandpass filters for 5G small-cell applications', IEEE Microw. Wirel. Compon. Lett., 2018, 28, (12), pp. 1110–1112, doi:10.1109/LMWC.2018.2871306.
51. Z. Yang, D. Psychogiou and D. Peroulis, "Design and Optimization of Tunable Silicon-Integrated Evanescent-Mode Bandpass Filters," in IEEE Transactions on Microwave Theory and Techniques, vol. 66, no. 4, pp. 1790-1803, April 2018, doi: 10.1109/TMTT.2018.2799575.
52. E. Elsaidy, A. Barakat, A. B. Abdel-Rahman, A. Allam and R. K. Pokharel, "Ultracompact CMOS 60-GHz Tapped-Line Combline BPF with Two Transmission Zeros Using Defected Ground Structures," in IEEE Transactions on Components, Packaging and Manufacturing Technology, vol. 8, no. 9, pp. 1642-1649, Sept. 2018, doi: 10.1109/TCPMT.2018.2861411.
53. L. -P. Li, J. -Y. Ding and X. -W. Sun, "Compact on-chip bandpass filter with low insertion loss for 60-GHz SIP application," 2018 Symposium on Design, Test, Integration & Packaging of MEMS and MOEMS (DTIP), Rome, Italy, 2018, pp. 1-3, doi: 10.1109/DTIP.2018.8394211.
54. R. Gómez-García, J. -M. Muñoz-Ferreras and D. Psychogiou, "Dual-Behavior Resonator-Based Fully Reconfigurable Input Reflectionless Bandpass Filters," in IEEE Microwave and Wireless Components Letters, vol. 29, no. 1, pp. 35-37, Jan. 2019, doi: 10.1109/LMWC.2018.2884151.
55. Z. J. Hou et al., "A W-Band Balanced Power Amplifier Using Broadside Coupled Strip-Line Coupler in SiGe Bi CMOS 0.13 μm Technology," in IEEE Transactions on Circuits and Systems I: Regular Papers, vol. 65, no. 7, pp. 2139-2150, July 2018, doi: 10.1109/TCSI.2017.2779174.
56. Anwesha Choudhury, Santanu Maity," Design and fabrication of CSRR based tunable mechanically and electrically efficient bandpass filter for K-band application", International Journal of Electronics and Communications (2016), doi: http://dx.doi.org/10.1016/j.aeue.2016.11.021.
57. Guoan Wang, D. Thompson, E. M. Tentzeris and J. Papapolymerou, "Low-cost RF MEMS switches using LCP substrate," 34th European Microwave Conference, 2004., Amsterdam, Netherlands, 2004, pp. 1441-1444.
58. Zhang QX, Yu AB, Guo LH, Kumar R, Teoh KW, Liu AQ et al. Development of RF MEMS switch on flexible organic substrate with wafer Transfer Technology (WTT). In Proceedings - IEEE 56th

Electronic Components and Technology Conference. 2006. p. 523-527. 1645698. (Proceedings - Electronic Components and Technology Conference). doi: 10.1109/ECTC.2006.1645698.

59. Patil, S. B., Chu, V. & Conde, J. P. Performance of thin film silicon MEMS on flexible plastic substrates. Sens. Actuat. A-Phys. 144, 201–206 (2008), doi: https://doi.org/10.1016/j.sna.2007.12.022.
60. Pestana, T. G. et al. Fabrication and characterization of thin-film silicon resonators on 10 mu m-thick polyimide substrates. J. Micromech. Microeng. 30, 045007 (2020), DOI 10.1088/1361-6439/ab7262.
61. Zhang, Y.-F.; Cui, M.; Wu, D.-P. Design and Fabrication of a MEMS Bandpass Filter with Different Center Frequency of 8.5–12 GHz. Micromachines 2023, 14, 280. https://doi.org/10.3390/mi14020280.

